JVI Journals.ASM.org

Functional Implications of the Binding Mode of a Human Conformation-Dependent V2 Monoclonal Antibody against HIV

Brett Spurrier,[a] Jared Sampson,[a] Miroslaw K. Gorny,[b] Susan Zolla-Pazner,[b,c] Xiang-Peng Kong[a]

Departments of Biochemistry and Molecular Pharmacology[a] and Pathology,[b] NYU School of Medicine, New York, New York, USA; Veterans Affairs New York Harbor Healthcare System, New York, New York, USA[c]

ABSTRACT

Data from the RV144 HIV vaccine trial indicated that gp120 V2 antibodies were associated with a lower risk of infection; thus, the mapping of V2 epitopes can contribute to the design of an effective HIV vaccine. We solved the crystal structure of human monoclonal antibody (MAb) 2158, which targets a conformational V2 epitope overlapping the α4β7 integrin binding site, and constructed a full-length model of V1V2. Comparison of computational energy stability to experimental enzyme-linked immunosorbent assay (ELISA) results identified a hydrophobic core that stabilizes the V2 region for optimal 2158 binding, as well as residues that directly mediate side chain interactions with MAb 2158. These data define the binding surface recognized by MAb 2158 and offer a structural explanation for why a mismatched mutation at position 181 (I181X) in the V2 loop was associated with a higher vaccine efficiency in the RV144 clinical vaccine trial.

IMPORTANCE

Correlate analysis of the RV144 HIV-1 vaccine trial suggested that the presence of antibodies to the second variable region (V2) of HIV-1 gp120 was responsible for the modest protection observed in the trial. V2 is a highly variable and immunogenic region, and structural information on its antigenic landscape will be important for rational design of an effective HIV-1 vaccine. Using X-ray crystallography, computational design tools, and mutagenesis assays, we carried out a detailed and systematic investigation of the epitope recognition of human V2 MAb 2158 and demonstrated that its epitope region overlaps the integrin binding site within V2. In addition, we propose a structure-based mechanism for mismatching of the isoleucine at position 181 and the increased vaccine efficacy seen in the RV144 vaccine trial.

HIV is among the most genetically variable human pathogens, and it is widely believed that a preventative vaccine must elicit antibodies that block infection by diverse strains of the virus. Thus, a detailed understanding of conserved structural elements of the epitopes recognized by cross-reactive, protective HIV-specific antibodies is an important step in vaccine design and development.

Data from the 2009 phase III RV144 vaccine clinical trial indicated that high levels of antibodies targeting the V2 region correlate with a lower risk of infection (1–3), suggesting that information about the epitopes in V2 will be important to the design of an effective vaccine. V2 is an immunogenic region of gp120, yet its heavy glycosylation and variable length are two reasons that V2 is known to contribute to increased antibody neutralization resistance (4, 5). Despite these escape mechanisms, antibodies to the V2 region are known to be highly cross-reactive (6, 7), and V2 is thought to have structurally and functionally conserved elements that may be targets for vaccine design (8–10). For instance, though this is still controversial (11), it has been suggested that during the early stages of viral infection, α4β7 integrin, which is highly expressed in gut-associated lymphoid tissue (GALT), mediates gp120 binding to host cells through a conserved integrin binding motif, LDI/V, within V2 (12–14). Recent data on a panel of mouse monoclonal antibodies (MAbs) targeting a region overlapping the integrin binding site have demonstrated that they can inhibit α4β7 binding (15). Therefore, antibodies whose epitopes overlap the α4β7 binding site in V2 might lower the probability of infection (16, 17), and the integrin binding mechanism could provide one explanation for the modest protection afforded in the RV144 vaccine trial (3, 9). In addition, electron tomography and cryo-electron microscopy (cryo-EM) studies have revealed that V1V2 is located at the apex of the unliganded trimer and is accessible to anti-V2 antibodies, thus suggesting that antibodies to V2 can bind the Env spike and play a role in inhibiting HIV infection (18–23).

There are three known epitope types in the V2 region. The first type, the V2q type, is defined by human MAbs, including 2909, PG9, PG16, CAP256, and CH01, that target quaternary neutralizing epitopes (hence the name V2q) preferentially present on the native trimeric spike (24–27). Crystal structures of scaffolded V1V2 molecules (from clade C strains CAP45 and ZM109) complexed with MAbs PG9 and PG16 showed that V1V2 can form an integral four-stranded beta sheet of the Greek key motif (beta strands A, B, C, and D), with V1 stemming from a disulfide bond between the two middle strands (strands A and B) (28, 29). Epitopes recognized by PG9 and PG16 are composed primarily of main chain positions 167 to 171 in strand C (strain HxB2 numbering) of V2. Both MAbs also make large contacts with a highly

Received 25 October 2013 **Accepted** 17 January 2014
Published ahead of print 29 January 2014
Editor: W. I. Sundquist
Address correspondence to Xiang-Peng Kong, xiangpeng.kong@med.nyu.edu.
Supplemental material for this article may be found at http://dx.doi.org/10.1128/JVI.03153-13.

doi:10.1128/JVI.03153-13

conserved N-linked glycan at residue N160 and another N-linked glycan, at either N156 (CAP45) or N173 (ZM109). However, a loop of 14 (for CAP45) or 16 (for ZM109) amino acids in V2, starting from the α4β7 integrin binding site (residues 179 to 181), could not be visualized in the structures of PG9- and PG16-bound molecules, because of missing electron densities (22, 23).

The second type of V2 epitopes, the V2p type, is defined by two human MAbs, CH58 and CH59, recently isolated from B cells of an RV144 vaccinee, which bind V2 peptides (30, 31). The epitopes for CH58 and CH59 were first mapped via alanine scanning mutagenesis to a region of V2 overlapping the region in beta strand C of V2 that is also part of the epitope recognized by MAbs PG9 and PG16. However, unlike the V2q-specific MAbs, both CH58 and CH59 bind monomeric gp120, are glycan independent, and, as noted, bind V2 peptides. Crystal structures of antigen-binding fragments (Fabs) of CH58 and CH59 in complex with a V2 peptide showed that the epitope of CH58 consists of a short α-helix, while that of CH59 has a coiled region followed by a 3_{10} helical turn (30). The data demonstrated that the region recognized by the V2q MAbs and the V2p MAbs includes residues 168 to 173; however, the conformations that they recognize differ: PG9 and PG16 bind to this region as a β-strand, while CH58 and CH59 bind to this region as an α-helix or a coil.

A panel of conformation-dependent epitope MAbs, including MAb 2158, define the third type of V2 epitopes, the V2i type (7). Although a crystal structure of one of these, MAb 697-30D, in its uncomplexed form, was determined recently, no structures of V2i-specific MAbs complexed with their cognate epitopes have yet been published. Mutagenesis studies and competition enzyme-linked immunosorbent assays (ELISAs) indicate that the epitopes recognized by this class of MAbs overlap the putative α4β7 integrin binding site motif (^{179}LDI/V^{181}), thus the name V2i, and this motif is spatially located on the opposite side from where the epitopes of PG9 and CH58 are located, in an unresolved region in the scaffolded V1V2 crystal structures (7, 22, 23, 32, 33). A recent study of the immunologic activity of a panel of seven V2i MAbs (including 2158) with gp120 molecules from 21 HIV strains demonstrated that these MAbs are highly cross-reactive with gp120s from diverse clades, and they recognize conserved antigenic determinants in V2 despite the sequence variability in the V2 regions of these molecules (7). To date, little is known about the structure of the epitopes recognized by the V2i MAbs.

Here we report a crystal structure of the Fab of the anti-V2i MAb 2158 and a detailed computational and mutagenesis analysis of its epitope. MAb 2158 was isolated from a subtype B virus-infected subject and is broadly cross-reactive and capable of neutralizing many tier 1 viruses (5, 7). However, it does not neutralize tier 2 viruses, even though it can bind quite a few tier 2 gp120s; an increased length of V2 and increased total number of glycosylation sites within the hypervariable region are possibilities for the discordance between 2158 binding and neutralization (7). Our structural analysis of Fab 2158, in concert with computational modeling and mutagenesis data, indicate that its binding mode involves a conformation-dependent epitope which is stabilized by a hydrophobic core in V2. Our results provide a binding motif signature for anti-V2i MAb 2158 and other members of the V2i MAb family and offer a structural explanation for the immunologic pressure on V2 observed in the RV144 clinical trial, i.e., why replacement of the isoleucine residue at position 181 in V2 is associated with a higher vaccine efficiency (34).

MATERIALS AND METHODS

Antibody and Fab preparation. Human MAb 2158 was produced as described previously (5, 35). Briefly, peripheral blood mononuclear cells from an HIV-1-infected individual were transformed with Epstein-Barr virus; those cells that were producing antibodies reactive with a murine leukemia virus (MLV) gp70-V1V2$_{\text{Case-A2}}$ fusion protein were fused with the human × mouse heteromyeloma SHM-D33 (36). The resulting hybridomas were cloned at limiting dilutions until monoclonality was achieved. MAb 2158 belongs to the IgG1 subclass and bears a kappa light chain (7).

To produce the antigen binding fragment, papain (Worthington) was activated with 10 mM cysteine and incubated with MAb 2158 at a 1:20 weight ratio for 1 h at 37°C. The reaction was quenched by adding iodoacetamide, and the Fc fragment was removed by passing the digestion product over a protein A column. The Fab was further purified by size-exclusion chromatography after dialysis overnight against 20 mM Tris (pH 6.8), 100 mM NaCl. The resulting Fab was aliquoted, flash frozen, and stored at −80°C.

Crystallization, data collection, structure determination, and refinement. For protein crystallization, Fab 2158 was concentrated to 15 mg/ml and screened against 288 crystallization conditions by using a TTP LabTech Mosquito crystallization robot. Final crystals were grown using the vapor diffusion method at 23°C by mixing 0.15 μl of protein with 0.15 μl of 23.5% polyethylene glycol 4000 (PEG 4000)–0.17 M ammonium sulfate–15% glycerol. Diffraction data were collected at beamline GM/CA-CAT at the Advanced Photon Source (APS), Argonne National Laboratory. The data were processed using MosFilm (37), with a high-resolution cutoff of 2.8 Å, determined by a combination of statistics, including I/σ, completeness, and correlation coefficients defined by Karplus and Diederichs (38). The structure was determined by molecular replacement using the structure of Fab 412d (PDB ID 2QAD) selected by BLAST (39). A solution was found using Phaser (40), and the model was refined with iterations of refinement by Phenix Refine (41) and manual adjustment by Coot (42).

Computational analysis of the antigen binding site of Fab 2158. The ICM optimal docking area (ODA) function was used to identify regions of Fab 2158 likely involving in antigen-antibody interactions. The algorithm identifies surface patches with low levels of desolvation energy based on atomic solvation parameters adjusted for protein-protein interactions (43). It has been benchmarked on a panel of nonhomologous proteins involved in nonobligate protein-protein interactions. The ICM PocketFinder function was used to identify potential binding pockets on the surface of Fab 2158. The algorithm builds a grid map of the van der Waals potential, and the position and size of the antigen binding pocket are determined based on the construction of equipotential surfaces after a smoothing transformation of the map emphasizes buried continuous regions of low potentials (44).

Computational model building of full-length V1V2. We built full-length V1V2 models using Rosetta 3.4's homology and loop-modeling applications as previously described (45). Briefly, the V1V2 sequences were threaded over the coordinates of the 1FD6 scaffolded-V1V2 template structure (PDB ID 3U4E), with the scaffold region removed, using the Rosetta 3.4 comparative modeling application. Rosetta 3.4's loop-modeling application was then used to model *de novo* the region missing in the template structure. Full atom relaxation was performed, resulting in at least 45,000 to 100,000 decoy models per sequence. The models were generated without the incorporation of glycans, because the Rosetta energy score function does not account for large intraresidue interactions with posttranslational modifications, such as N-linked glycosylation. The decoy models were scored and clustered according to the root mean square deviation (RMSD), and a final model for each sequence was chosen as the lowest-scoring decoy model that was a member of the largest cluster. Structural figures were drawn using PyMol (Schrödinger, LLC).

Computational stability analysis. To computationally calculate the energy difference between a wild-type V1V2 model (CAP45 sequence)

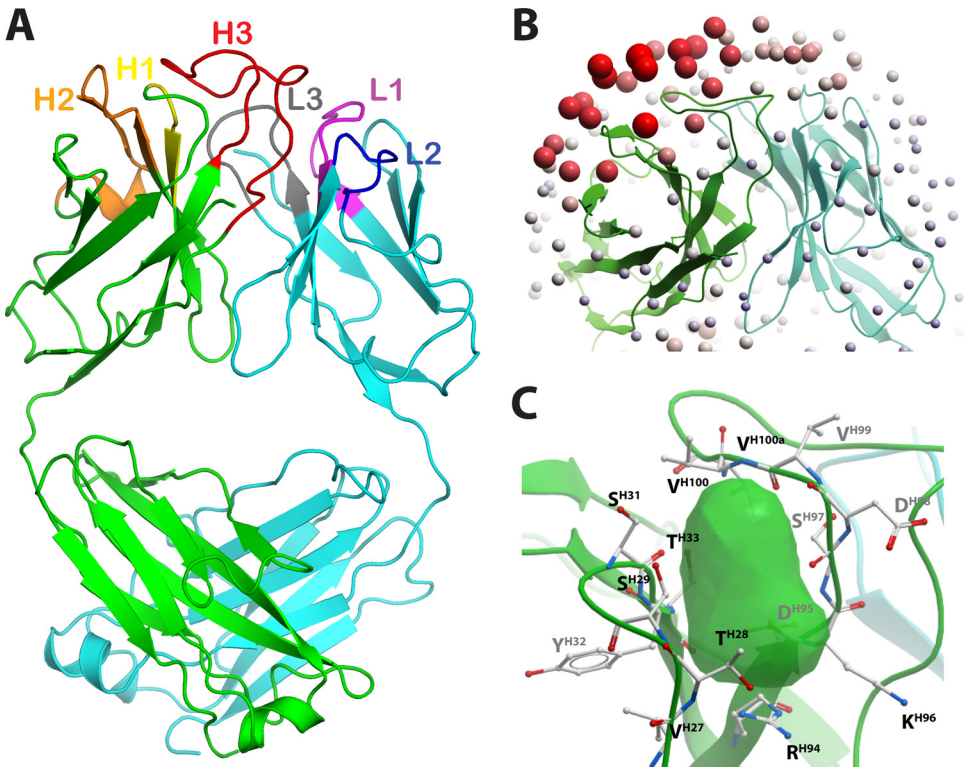

FIG 1 Crystal structure of Fab 2158. (A) Ribbon representation of the structure of Fab 2158 in a side view. The light and heavy chains are colored cyan and green, respectively, and the CDR loops are colored differently. (B) ODA analysis of Fab 2158. ODA uses a desolvation energy calculation to predict the regions on Fab 2158's surface which are likely to be involved in protein-protein interactions. The redness and size of the spheres are proportional to the most favorable desolvation score at each particular location. ODA analysis of Fab 2158 suggests that protein-protein interactions are likely to occur predominantly around the heavy chain. (C) Surface pocket. A single surface pocket, between CDR H1 and CDR H3, was found by ICM PocketFinder. The pocket is created by residue side chains (residues labeled in black) as well as residue backbones (residues labeled in gray).

and a panel of V1V2 mutant models, we independently replaced every residue in V1V2 (positions 132 to 199) with each of the possible 20 amino acids. We used the Rosetta 3.4 backrub application to minimize both the side chain of the mutated residue and the local backbone (46). We then scored the mutant structure and subtracted its energy score by the wild-type energy score. These data yielded differences in computational Gibbs energy ($\Delta\Delta G$) between our panel of mutant models and the wild-type model that can imply the conformational changes induced by a particular mutation at each position of V1V2.

Site-directed mutagenesis. The plasmid of VRC8400 containing the construct of 1FD6 scaffolded V1V2 (CAP45 sequence) was obtained from Peter Kwong (VRC, NIH), and it contains an artificial N-terminal secretion signal and a C-terminal HRV3C recognition site followed by an 8-His tag and a Streptag-II marker (28). Point mutations were introduced into the construct by using a QuikChange II XL site-directed mutagenesis kit (Stratagene, La Jolla, CA) according to the manufacturer's instructions. All mutant constructs were sequenced to confirm the correct amino acid changes.

Protein production in 293S cells and ELISA. Mutation constructs were transiently transfected into HEK 293S GnTI$^{-/-}$ cells (47) in 24-well plates, and the cells were cultured for 72 h (28). The cell culture supernatant was collected, equally distributed among 6 wells of a Ni^{+}-coated 96-well plate (Pierce), and incubated overnight. The plates were washed in phosphate-buffered saline with 0.5% Tween 20 (PBST) three times before five of the six wells were incubated with MAb 2158 titrations overnight. The sixth well was incubated with IRDye total protein stain (Licor Biosciences) for 2 h. The plates were washed three times, and the wells coated with MAb 2158 primary antibody were incubated with an IRDye-800-conjugated anti-human secondary antibody (Licor Biosciences) for 2 h. The plates were washed again in PBST three times, and the fluorescence signal was read on a Licor Odyssey Clx near-infrared scanner. The 700-nm channel was used to capture the signals of the wells incubated with IRDye total protein stain (1 well per sample), and the 800-nm channel was used to capture the signals of the IRDye-800-conjugated secondary antibody (5 wells per sample). The signals were quantitated with ImageJ (http://rsbweb.nih.gov/ij), and the binding signal for each of the 5 wells per sample was normalized to the total protein signal for that sample. The 50% effective concentration (EC_{50}) of the titration curve was calculated using Prism (Graphpad Software, La Jolla, CA). Each mutant was repeated in triplicate. A wild-type sample was included in every plate as a positive control. Negative controls with primary antibody only, secondary antibody only, and empty wells were included in each 96-well plate used.

Protein structure accession number. Atomic coordinates and structure factors for the Fab 2158 structure have been deposited in the RCSB Protein Data Bank under ID code 4OAW.

RESULTS

Structure determination and analysis of Fab 2158. The antigen-binding fragment (Fab) of MAb 2158 was crystallized in its uncomplexed state, and its structure was determined and refined to 2.8-Å resolution (Fig. 1A and Table 1). Fab 2158 crystallized in the trigonal space group $P3_2$, with two Fabs in the asymmetric unit (ASU); they were highly similar, with an RMSD of 0.22 Å when their C-α atoms were superimposed. For clarity, we refer to only one of the Fabs, and we follow the Kabat and Wu numbering conventions, with residue numbers of the heavy and light chains preceded by "H" and "L," respectively (48).

TABLE 1 Data collection and refinement statistics

Parameter	Value or description for Fab 2158[a]
Data collection statistics	
Wavelength (Å)	1.033
Space group	$P3_2$
Cell dimensions	
a, b, c (Å)	73.71, 73.71, 215.95
α, β, γ (°)	90, 90, 120
Resolution (Å)	215–2.8 (2.89–2.8)
R_{sym}	0.23 (0.95)
CC*[b]	0.95 (0.62)
$CC_{1/2}$	0.98 (0.48)
I/σ	5.6 (1.8)
Completeness (%)	99.6 (99.5)
Redundancy	5.6 (5.5)
Refinement statistics	
No. of unique reflections	31,988 (3,227)
Resolution	2.8–54.83 (2.8–2.9)
R_{work}/R_{free}	0.18/0.25
No. of atoms	
Protein	6,786
Ligand	47
Water	164
RMSD	
Bond lengths (Å)	0.010
Bond angles (°)	1.309
Ramachandran plot statistics (%)	
Favorable and allowed regions	99.1
Outliers	0.9

[a] Values in parentheses are for the highest-resolution shell.
[b] CC* and $CC_{1/2}$ are correlation coefficients defined in reference 38.

The long complementarity-determining region (CDR) H3 loop of Fab 2158 (21 amino acids by the Kabat definition) forms a sharp, ~90° bend at base residues D^{H98} and Y^{H100i}, resulting in an overall rounded hydrophobic surface. A four-valine motif stretches along the N-terminal side of the CDR H3 loop, from V^{H99} to V^{H100b}, with the backbone of V^{H100b} making a hydrogen bond with T^{H52} in CDR H2, thus helping to hold CDR H3's conformation in a laid-back rounded presentation (Fig. 1). The side chain of I^{H100e} also helps to stabilize the positioning of the CDR H3 loop by participating in hydrophobic packing with Y^{H100j}, P^{H100g}, and part of Y^{L91}. The aforementioned four consecutive valines align on one side of the CDR H3 loop, and they, together with three residues from the adjacent CDR H2 loop (I^{H53}, F^{H54}, and I^{H56}), form a hydrophobic patch on the surface of its antigen binding site (paratope). There are also solvent-exposed amino acids (D^{H98} and R^{H100f}) that may mediate charge interactions between MAb 2158 and its epitope. This antigen-binding surface is quite different from those of other MAbs targeting the V2 region. For instance, the CDR H3 loops of the V2q MAbs PG9 and PG16 contain 25 amino acids and form a "hammerhead" subdomain (28, 49, 50), which is surface exposed and negatively charged. Two other V2q MAbs, 2909 and 2.5B, also have long, extended, negatively charged CDR H3 loops (51), which, again, are in contrast to that of Fab 2158. The V2p MAbs CH58 and CH59, derived from an RV144 vaccinee, lack a long CDR H3 loop but still possess a highly negatively charged surface (30).

Computational tools were used to analyze the paratope of MAb 2158 and to predict its modes of interaction with its epitope. First, we used the ICM ODA tool to predict regions of protein-protein interactions (43). ODA had previously correctly identified the paratope of anti-V3 antibodies (51). Application of ODA to MAb 2158 indicated that the hydrophobic patches of the H2 and H3 CDR loops dominated the antigen-antibody interactions (Fig. 1B). Individual residues contributing the highest binding potentials included CDR H1 residues S^{H30} and S^{H31}, CDR H2 residues I^{H53}, I^{H54}, and I^{H56}, and CDR H3 residues V^{H100}, V^{H100b}, and T^{H100c} (data not shown).

Potential binding pockets in the paratope of MAb 2158 were identified using the ICM PocketFinder algorithm (44), which searches the surface for binding pockets by calculating the van der Waals potential along the antibody surface and then applying a smoothing function to visually identify pockets. PocketFinder located one pocket, between CDRs H1 and H3. This pocket has a volume of ~220 $Å^3$ and is flanked by residues from CDR H1 (V^{H27}, T^{H28}, S^{H29}, S^{H31}, Y^{H32}, and T^{H33}) and CDR H3 (R^{H94}, D^{H95}, K^{H96}, S^{H97}, D^{H98}, V^{H99}, V^{H100}, and V^{H100a}). While the residues comprising the sides of the pocket are primarily hydrophobic, the base of the pocket is formed by a positively charged arginine, R^{H94} (Fig. 1C); thus, this pocket can accommodate the side chain of a negatively charged V2 residue.

Recently, we solved the Fab structure of another V2i MAb, 697-30D (7), which has several structural similarities with MAb 2158. Both MAbs present a convex antigen binding region, and structural alignments of the backbone of the 697-30D heavy chain with that of the 2158 heavy chain showed a pairwise RMSD of 1.9 Å (excluding CDR H3). ODA analysis of 697-30D also suggests that the heavy chains dominate interactions with its epitope (7). These data suggest that MAbs 2158 and 697-30D belong to the same family of antibodies and interact with V1V2 through hydrophobic interactions, in direct contrast to the binding modes of V2q MAbs PG9 and PG16 and V2p MAbs CH58 and CH59.

Computational modeling of the V1V2 structure. Because previous data have suggested that the epitopes recognized by V2i MAbs involve a discontinuous matrix of residues, including five amino acids (7, 32, 33) within the unresolved region in the V1V2 crystal structures (28), we employed computational homology and loop-modeling methods to build *de novo* this region for the CAP45 V1V2 sequence (Fig. 2A and B). We generated this model by taking into account the conditions of *de novo* loop modeling: longer loops require larger conformational sampling space due to an increase in the conformational degrees of freedom. Our full V1V2 model required modeling of loops ranging from 14 amino acids, so we extended the sample space by generating 100,000 Rosetta decoy models (52, 53). In addition to the full-length V1V2 model for strain CAP45, we also generated one for ZM109 and another 20 sequences of strains tested in a previous study (7), and the results are consistent with what we present here for the CAP45 model (data not shown).

The minimum energy conformation for our model with the fully *de novo* modeled loop (residues 177 to 191) shows that this loop connects β-strands C and D in an elongated fashion, with the sequence-variable region (residues 188 to 190e) forming a short loop extending into the solvent. The F176 side chain orients toward the structural hydrophobic core of V1V2, and the side chain of Y177 orients toward the solvent (Fig. 2C). The side chain of D180 also orients toward the solvent, while the side chain of V181 points toward the hydrophobic core. Previous data suggested that both Y191 and L193 affect the reactivity of MAb 2158 and other

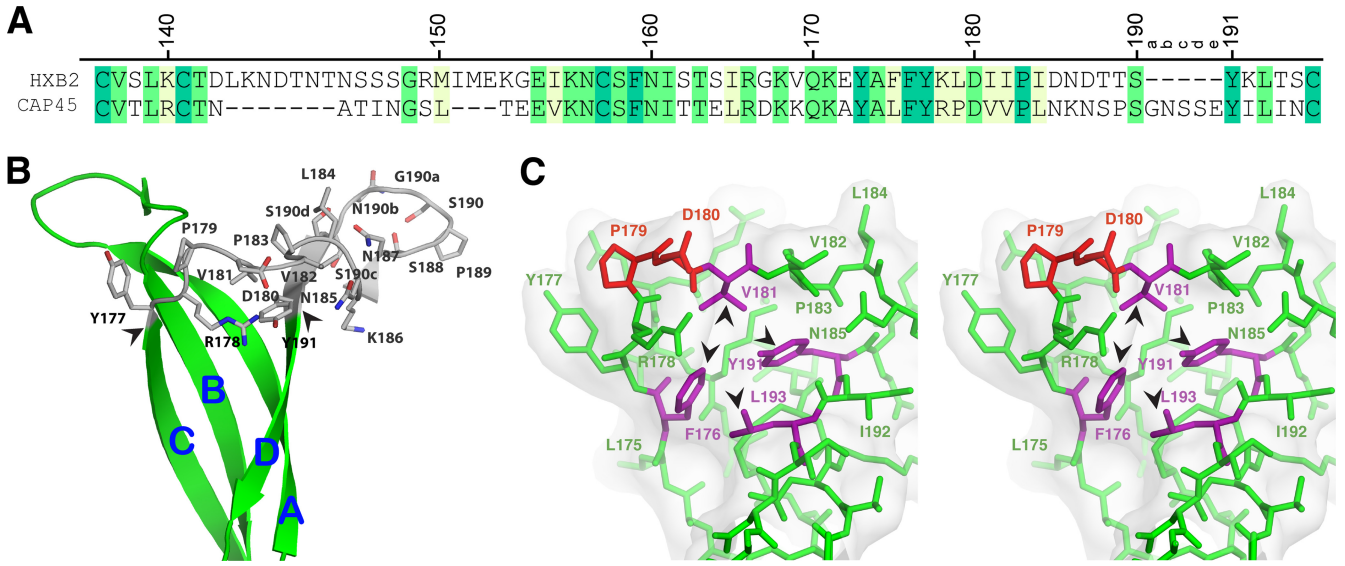

FIG 2 Computational model of V1V2. A full-length V1V2 model of the CAP45 sequence was built, based on the crystal structure in complex with PG9 (28), by *de novo* modeling of the loop region missed in the crystal structure. (A) Residue numbering of CAP45. The sequence was aligned with that of HxB2 and numbered accordingly. (B) Cartoon representation of the V1V2 model. The *de novo*-modeled region from Y177 to Y191 is colored gray, with the side chains shown as sticks. (C) Stereoview of the hydrophobic core in the V1V2 model. All residues are shown as green sticks, except for the residues of the hydrophobic core, i.e., F176, V181, Y191, and L193, which are colored purple (black arrows), and residues P179 and D180, part of the integrin binding site, which are colored red.

V2i MAbs (32, 33), and our model has these two residues' side chains pointing toward the hydrophobic core of the V2 loop. Thus, our model suggests that there are two groups of residues that can affect the antigen binding of 2158: (i) contact residues, whose side chains mediate direct antibody-antigen interactions; and (ii) noncontact residues, which stabilize V2 in the optimal conformation for MAb 2158 binding.

Computational energy analysis of V2 point mutations. In order to gain guidance for our experimental mutagenesis investigation of the epitope recognized by MAb 2158, we first carried out systematic *in silico* mutagenesis analyses. Using our CAP45 V1V2 model (Fig. 2), every residue in V1V2 was computationally mutated to each of the 20 amino acids, and the computational energy differences between the mutant models and the wild-type model were calculated ($\Delta\Delta G = \Delta G_{\text{Mutant}} - \Delta G_{\text{Wild-type}}$) (see the supplemental material for details). A large $\Delta\Delta G$ value for a point mutation indicates that the structure will likely undergo a conformational change relative to the wild type. Conversely, a small $\Delta\Delta G$ value suggests that the mutant structure will maintain a conformation similar to that of the wild type (46). Several residues had small mutation $\Delta\Delta G$ values. For example, all mutations of D180, the second residue of the integrin-binding tripeptide, had small $\Delta\Delta G$ values, ranging from -1.5 to $+1.3$ Rosetta energy units (REU), with the exception of the D180P mutation (which never occurs in nature in HIV-1 sequences; $\Delta\Delta G = 12.3$ REU). This suggests that the structure is energetically stable with all nonproline mutations. Likewise, mutations with low $\Delta\Delta G$ values at position 179, the first residue of the integrin binding site, also suggest structural stability for this position. Similarly, when V181 was mutated to isoleucine, a common amino acid at position 181, the $\Delta\Delta G$ value was 0.1, suggesting structural stability. However, there were mutations that resulted in large $\Delta\Delta G$ values. Several mutations, including those at F176, V181, Y191, and L193, had consistently high $\Delta\Delta G$ values for all *in silico* mutations, and their side chains are all oriented toward the hydrophobic core of V2 in our model (Fig. 2C). Mutations of such residues likely alter the conformation of V1V2 and may disrupt the epitope presentation for MAb 2158. Using these data, a panel of mutations to be tested *in vitro* was designed (Table 2).

Experimental mapping of MAb 2158's epitope through site-directed mutagenesis. To further map the epitope of MAb 2158, we performed a series of site-directed point mutations on scaffolded V1V2 (CAP45 sequence) (28) and compared the mutants' ELISA binding to MAb 2158 with that of the wild type. Mutations were initially chosen from our list of computational $\Delta\Delta G$ energies, with additional mutations made based on other factors (Table 2). For clarity of discussion, we have grouped the V2 mutations into four categories according to their structural locations (Fig. 3): (i) strands B and C (positions 160 to 171), (ii) strand C tail (positions 172 to 175), (iii) the integrin binding site (positions 179 to 181), and (iv) the sequence-variable region and strand D (positions 183 to 193).

Point mutations made in the strand B-C region had varied effects on MAb 2158 binding. We first tested MAb 2158's binding dependency on N160 and I161, located at the N terminus of this region, by independently introducing N160K and N160K/I161V mutations. Both mutants showed no loss of binding compared to the wild type. When we introduced a charge opposition at position 168, in the middle of this region, by using the K168E mutation, only 6% of binding was retained compared to that of the wild type, whereas K168L and K168V mutants retained 48% and 52% of wild-type binding, respectively. When the positive charge was kept by use of a K168R mutation, MAb 2158 binding almost matched the wild-type binding level. Mutation of K169 to methionine did not change the binding of MAb 2158 relative to that of the wild type, but when K169L and K169G mutations were introduced independently, the binding was reduced to 53% and 42%, respectively. Mutations at the end of this region, i.e., Q170K,

TABLE 2 V1V2 mutations and their rationales

Position	CAP45 residue	Mutated residue	ΔΔ*G* (REU)	Commonality (%)[a]	Rationale
160	N	K	0.22	2.28	Loss of glycan; SF162 sequence at this position
160 + 161	NI	KV		0.81	Loss of glycan; double mutation
168	K	E	0.23	0.75	Charge opposition
		L	−0.11	0.03	Stable amino acid substitution[b]
		V	0.44	0.08	Stable amino acid substitution
		R	0.56	10.94	Same charge; stable amino acid substitution
		Q	−0.07	0.46	Stable amino acid; common at position 169
169	K	M	−0.14	9.89	Common amino acid in clade B
		L	1.82	1.55	Loss of charge
		G	3.03	0.31	Loss of side chain
		Q	2.12	5.97	Common amino acid in clade AE
170	Q	K	1.03	28.03	Common amino acid
171	K	S	−0.12	0.83	Stable amino acid substitution
		R	0.45	7.90	Stable amino acid substitution
172	A	E	0.96	44.10	Common amino acid; stable amino acid substitution
173	Y	N	1.91	2.57	Introduction of glycan when L175T mutation is present
		R	2.06	2.35	Introduction of charge
174	A	L	1.95	0.00	Larger side chain; less stable
175	L	T	1.79	1.34	Introduction of glycan when T173N mutation is present
173 + 175	Y/L	N/T		0.06	Introduction of glycan at N173
179	P	L	0.48	79.95	Most common amino acid
		Q	0.41	0.23	Naturally occurring but uncommon amino acid
		R	0.25	0.00	Charge introduction
180	D	S	0.13	0.00	Loss of charge; stable amino acid substitution
		E	0.86	0.00	Same charge as aspartic acid; stable amino acid substitution
		G	−0.26	0.00	Loss of side chain; stable amino acid substitution
181	V	G	4.67	0.00	Loss of side chain; large instability
		R	5.69	0.00	Introduction of a charge; large instability
		I	0.10	6.79	Most common amino acid; stable amino acid substitution
183	P	D	3.86	0.03	Introduction of a charge; large instability
185	N	D	4.08	40.89	Large instability
		R	−0.54	0.54	Stable amino acid substitution
186	K	D	0.16	17.18	Stable amino acid substitution
190b	N	Y	−0.44	0.00	Stable amino acid substitution
		T	4.56	0.00	Large instability
S190d	S	A	2.23	0.00	Loss of preceding N-linked glycan
191	Y	G	7.27	0.00	Loss of side chain; repeat mutation from reference 32
193	L	G	5.15	0.00	Loss of side chain; repeat mutation from reference 32

[a] Occurrence of mutation within the Los Alamos National Laboratory HIV sequence database.
[b] With small ΔΔ*G* values.

K171S, and K171R mutations, did not abrogate 2158 binding, and in the case of Q170K and K171R mutations, binding was increased over that of the wild type, to 157% and 126%, respectively (Fig. 3A).

We then introduced mutations in the strand C tail segment of V2, which again mediated various levels of influence on MAb 2158 binding. The Y173N and L175T point mutations resulted in minimal changes in MAb 2158 binding, retaining 71% and 86% of the wild-type binding level, respectively, while A172E and A174L mutants displayed decreases in binding, to 34% and 7%, respectively. Although an N-linked glycan at position 173 occurs in approximately 1% of sequences (http://www.hiv.lanl.gov/), we saw that introducing a glycosylation signal at this position (by introducing combined Y173N and L175T mutations) in the CAP45 construct

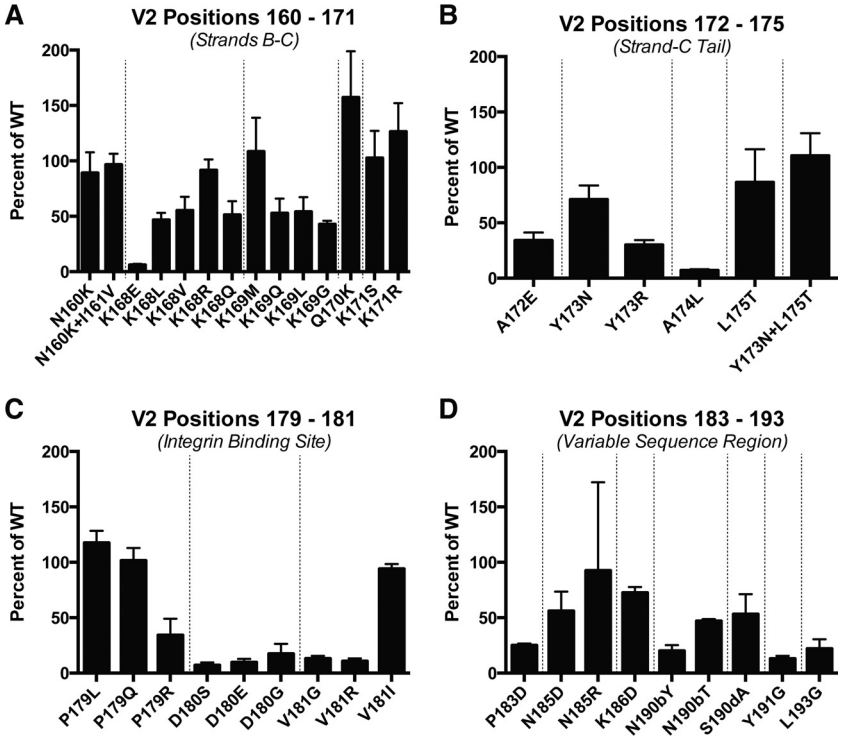

FIG 3 MAb 2158 binding of V2 mutants. Point mutations were introduced into the 1FD6 scaffolded V1V2 (CAP45 sequence) and tested for binding with MAb 2158. Mutants were made to interrogate positions in the strand B-C region (residues 160 to 171) (A), the strand C tail region (residues 172 to 175) (B), the integrin binding site (residues 179 to 181) (C), and the variable sequence region (residues 183 to 193) (D). The ELISA result for each mutation is shown as a percentage of binding relative to that of the wild type (WT).

did not change MAb 2158's binding pattern relative to that of the wild type (Fig. 3B).

In contrast, point mutations at the integrin binding site of V2 drastically reduced binding. We first tested the commonly occurring amino acids. When P179 (an amino acid found in strain CAP45 but found infrequently in other strains) was mutated to the common amino acid leucine (P179L) and another naturally occurring HIV amino acid, glutamine (P179Q), binding with MAb 2158 was found to be 117% and 101% that of the wild type, respectively. However, P179R mutation (a nonnatural mutation which introduces both a charge and a non-HIV amino acid) reduced the binding to 34% of the wild-type level. We then looked at the highly conserved aspartic acid at position 180. When it was mutated to three different amino acids, by D180S, D180E, and D180G mutations, the binding was radically reduced, to 7%, 9%, and 17%, respectively. Likewise, V181G and V181R point mutations, located at a position recently noted to be important by the RV144 sieve analysis (34), also showed reductions in binding, to 13% and 10%, respectively, whereas mutation to the commonly occurring amino acid at this position, isoleucine (V181I), resulted in a binding level similar to that of the wild type (94% of wild-type level) (Fig. 3C).

The V2 region between amino acids 183 and 193 is highly variable (8), and mutations in this region had varied effects on MAb 2158 binding (Fig. 3D). A P183D mutation that introduced a negatively charged residue at this position reduced the binding to 25% of the wild-type level. However, position 185 had a better tolerance for charged residues, with N185D and N185K mutations resulting in 50% and 92% binding, respectively. Similarly, the K186D mutant displayed a minimal reduction, to 72%. When the potentially glycosylated asparagine at position N190b was mutated to either tyrosine or threonine, the binding was reduced to 20% or 47%, respectively. We then mutated S190d, the third position of the tripeptide required for glycosylation at N190b, to alanine (S190dA), which showed a 53% retention of binding. These data suggest that 2158 binding is sensitive, but not critically, to the glycan at N190b. The mutations that we made at the N terminus of the D strand of the V2 beta sheet, i.e., Y191G and L193G mutations, also showed drastic decreases in 2158 binding, to 13% and 22%, respectively (Fig. 3D).

Taken together with our $\Delta\Delta G$ analysis, these mutagenesis data suggest that the binding of MAb 2158 is influenced by residues overlapping the integrin binding site, as well as a discontinuous set of residues throughout V2 (Fig. 4), although direct $\alpha 4\beta 7$-binding competition assays have not been performed. These residues can be separated into two groups. The first group consists of V2 residues with small $\Delta\Delta G$ values in computational mutagenesis (Table 2; see the supplemental material) and a loss of binding when probed by experimental mutagenesis, suggesting that amino acids at these positions make direct contact with MAb 2158 through side chain interactions. The representative residue in this group is D180, in the integrin binding site. The second group consists of V2 residues that, when mutated, show large computational $\Delta\Delta G$ values (Table 2; see the supplemental material), together with a loss of binding to MAb 2158, indicating that these residues stabilize the conformation of V2 and provide optimal exposure of the V2 contact residues which bind to MAb 2158; the latter residues may or may not also have direct contact with MAb 2158. The representa-

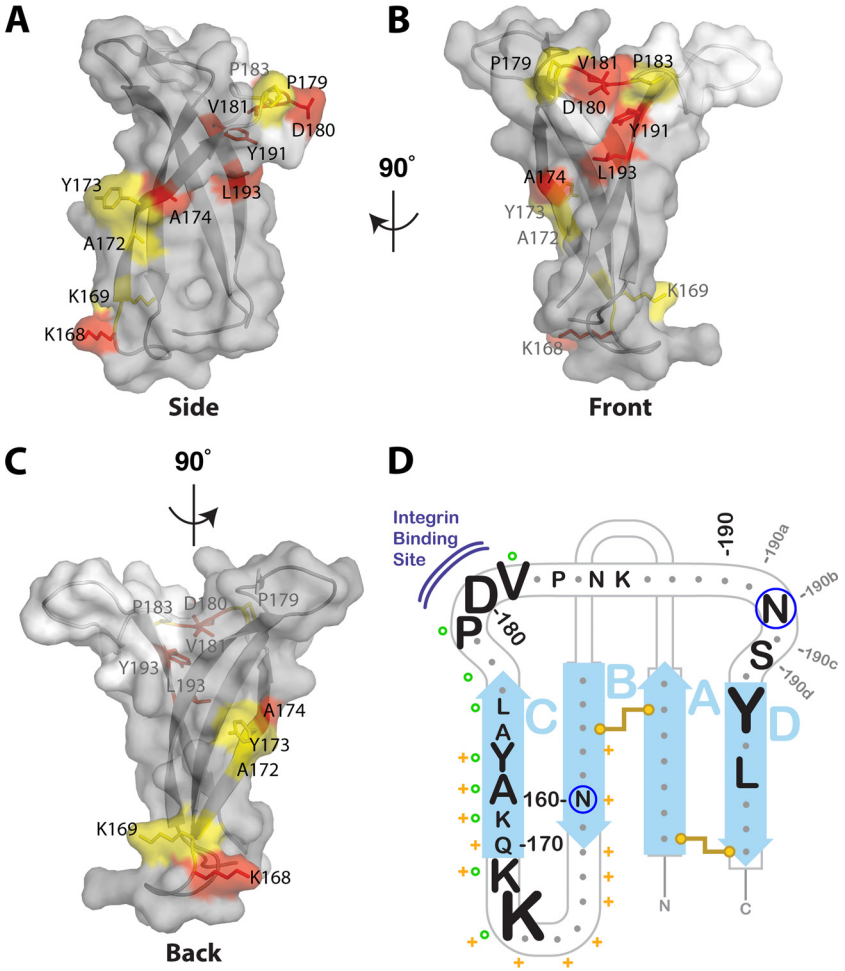

FIG 4 Mapping of mutagenesis binding data. A surface representation (partially transparent) of V1V2 is shown in three views: side (A), front (B), and back (C). The surfaces of the *de novo*-modeled amino acids at V2 positions 177 to 191 are shown in white, while the rest of the molecule is colored gray. Residues interrogated by mutagenesis were labeled and colored according to their mutants' ELISA binding to 2158: red for less than 15% binding relative to that of the wild type, and yellow for binding levels between 15% and 50%. Residues with mutations that showed minimal to no binding changes relative to the wild type were left uncolored. (D) V1V2 schematic diagram based on the crystal structure of the 1FD6 scaffolded V1V2 (CAP45 sequence) in complex with Fab PG9 (28). The four antiparallel beta sheets (blue arrows) are labeled A, B, C, and D, with V1 stemming from a disulfide bond between beta strands A and B. Amino acids of the residues interrogated in our mutagenesis study are shown with their sizes reflecting the mutation effects on 2158 binding, i.e., larger labels indicate that at least one mutation resulted in a larger inhibition of MAb 2158 binding to the mutated V1V2-scaffold protein, whereas smaller residue labels indicate no change relative to wild-type binding. For comparison, locations of the PG9 epitope are marked with yellow pluses, and those of the CH58 epitope are marked with green circles.

tive residue in this group is the integrin binding site residue 181, which is shown in our models to participate in forming the hydrophobic core of V2 (Fig. 2).

Model of integrin binding. Our model of the integrin binding motif in V2 is consistent with a recently published crystal structure of the α4β7 headpiece in complex with an I/LD mimetic, RO0505379 (1,6-dimethyl-2-oxo-4-trifluoromethyl-pyridine) (54). The structure shows that the molecule binds to a cleft between α4 and β7, with its carboxyl group mimicking an aspartic acid side chain, one oxygen coordinated by a bound metal (Mg^{2+}), and the other oxygen coordinated by the backbone of Y143 of β7 (Fig. 5A). The leucine mimic (or other small hydrophobic or polar residue) binds to a small hydrophobic pocket in β7. We docked our CAP45 V1V2 model *in silico* with the crystal structure of the α4β7 headpiece (Fig. 5B and C), showing that our *de novo*-modeled integrin binding motif fits into the groove between α4 and β7, with shape complementarity. Residues P179 and D180 make the largest contacts with the α4β7 headpiece, and the other residues between residues 179 and 187 make additional, minor contacts. Moreover, the positive charge at Arg^{H95} of Fab 2158, which forms the base of the primarily hydrophobic pocket, may partially mimic the positive charge of the Mg^{2+} ion seen binding to the aspartic acid mimic in the α4β7 headpiece crystal structure.

DISCUSSION

The V2 region of gp120 has gained attention recently because the RV144 correlate analysis suggested that the presence of anti-V2 antibodies reduces the risk of infection (2, 3). Unlike the case for several other immunogenic regions of gp120, structural information about V2 is only beginning to come to light, and additional structural information is necessary for the design of an effective vaccine targeting the V2 region. Here we solved the crystal struc-

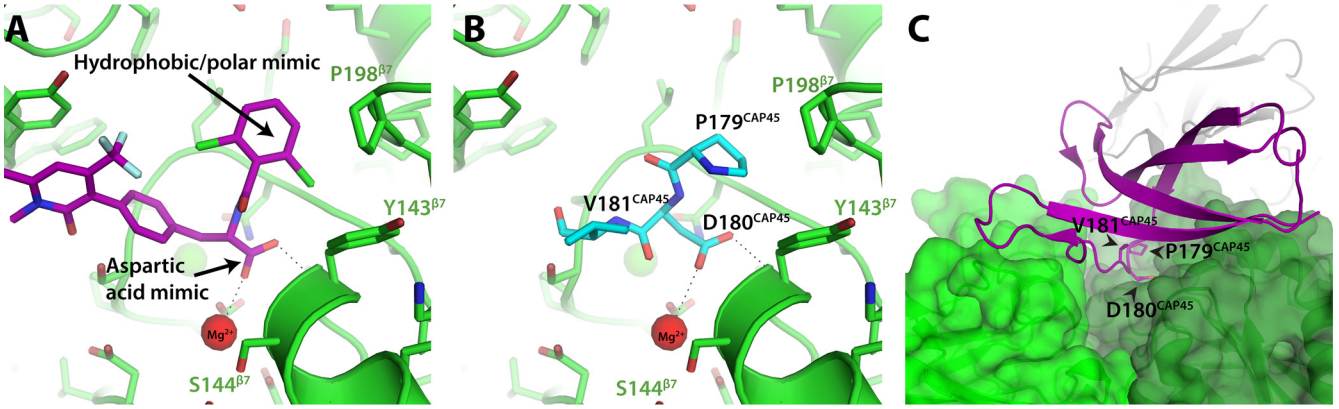

FIG 5 Docking of V1V2 model onto the α4β7 headpiece. (A) A small molecule, RO0505379 (purple), which mimics the common Ile/Leu-Asp amino acid motif (equivalent to ^{179}LD^{180}), in complex with the α4β7 integrin headpiece (green/dark green) and the Fab fragment of MAb Act-1 (PDB ID 3V4V). (B) The ^{178}PDV^{180} fragment (cyan) of our CAP45 V1V2 model (Fig. 2) was superimposed over the position of RO0505379, showing that the ^{178}PDV^{180} motif in CAP45 can interact with the α4β7 integrin headpiece in the same manner as that for RO0505379. (C) Side view of our full CAP45 V1V2 model docked *in silico* into the α4β7 integrin headpiece (the α4 subunit is shown in green, and the β7 subunit is shown in dark green) complexed with Fab Act-1 (gray and light gray; used in the crystallization to lock the α4β7 headpiece in the open conformation). The integrin binding site of V2 (black arrows) docks into the same conformation as the superposition of the PDV fragment with RO0505379 shown in panel B.

ture of the Fab fragment of human MAb 2158, specific for an epitope of the V2i type overlapping the integrin binding site, and used these data along with existing crystallographic data and modeling techniques to compare the different categories of V2-directed MAbs and the epitopes they recognize. The V2i-specific Fab 2158 displayed several properties in stark contrast to those of V2q MAbs, e.g., PG9, and V2p MAbs, e.g., CH58. The long CDR H3 loop of 2158 makes a sharp bend to form a convex hydrophobic surface. In contrast, V2q MAbs have a large, negatively charged, "hammerhead" CDR H3 subdomain, and V2p MAbs also have a negatively charged surface. Our analysis of Fab 2158 suggests that MAb 2158 binds V2 with residues mainly from the heavy chain, and a small pocket located between CDRs H1 and H3 may be involved in binding of a negatively charged side chain of an epitope residue. Thus, MAb 2158 binds V2 by using a surface comprised primarily of hydrophobic side chains. The nonspecific nature of these hydrophobic contacts may explain why MAb 2158 can react with gp120s from multiple clades (7).

Our structural modeling of the unresolved V2 region of residues 177 to 191 in the V1V2 crystal structures shows a hydrophobic core formed by F176, V181, Y191, and L193. To examine this further, we systematically calculated the computational energy differences between our V1V2 model and an array of computational mutants (see the supplemental material), allowing us to predict mutations that might either alter or retain the V2 conformation. This information was then used to choose structurally relevant mutants to clone, express, and test for binding by MAb 2158. The binding data (Fig. 3) and previously published data (32, 33) show that mutations in the same four residues, identified with high $\Delta\Delta G$ differences (residues 176, 181, 191, and 193), radically decrease binding by MAb 2158; the side chains of all four of these residues orient toward the core of the V2 structure (Fig. 2C). Our V1V2 model shows that F176 has a 135-Å^2 buried surface area in the V2 core, and the high $\Delta\Delta G$ value for its alanine mutant also indicates the likeliness that V2 may alter its conformation with the F176A mutation, correlating with a loss of binding shown in previous data (32, 33). Additionally, the loss of the large hydrophobic side chain of Y191, whose buried surface area was 112 Å^2 in our model, in the Y191G mutation resulted in almost complete MAb 2158 binding abrogation. Similarly, L193 has a 112-Å^2 buried surface area in the V2 core, and the loss of its side chain abrogated binding, again suggesting that L193 is a critical residue in stabilizing MAb 2158's epitope. Thus, both the modeling and binding data strongly suggest that residues 176, 181, 191, and 193 form a hydrophobic core essential for the structure and availability of the residues to which MAb 2158 binds.

These data are relevant to understanding the results of the sieve analysis of the V2 sequences of the breakthrough viruses in the RV144 clinical vaccine trial, which indicated that the vaccine was most effective if the isoleucine at position 181 of the vaccine was mismatched; a mismatch at position 181 resulted in a 78% estimated vaccine efficacy (34). In our structural model, the valine side chain that exists at position 181 in CAP45 contributes to the hydrophobic core, along with the side chains of F176, Y191, and L193. Residue V181 has a 94-Å^2 buried surface area, and our computational stability ($\Delta\Delta G$) analysis suggests that only smaller hydrophobic residues at position 181 are likely to maintain a stable structure (see the supplemental material). In particular, an *in silico* mutation of the commonly occurring amino acid, V181I, resulted in almost no change in computational energy over the wild-type valine in CAP45 ($\Delta\Delta G = 0.1$). Substituting an isoleucine at position 181 in our model showed that the mutant has a 122-Å^2 buried surface area in the hydrophobic core, representing a 28-Å^2 increase in the buried surface area. However, replacing residue 181 with a larger hydrophobic amino acid, such as leucine or methionine, was predicted not to be as stable ($\Delta\Delta G = 2.8$ for leucine and 3.4 for methionine). This suggests that the proportion of contacted surface area from an isoleucine at position 181 may be ideal for maintaining a tightly packed V2 conformation, and thus may be advantageous for the virus. In the case of RV144, when residue 181 is an amino acid mismatching the vaccine isoleucine residue, the V1V2 core will be loosely packed, potentially making the epitopes targeted by V2p antibodies more accessible. Thus, the virus became more vulnerable to antibodies induced in the RV144 study, and the structural modeling and binding data presented

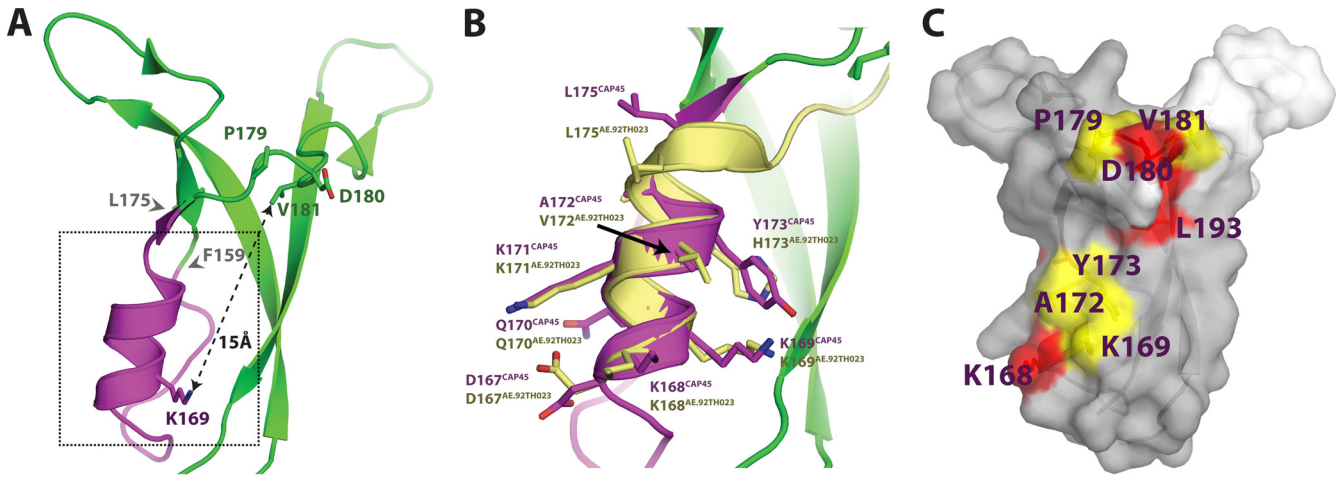

FIG 6 Alternative conformation of strand C region of V1V2. (A) We used Rosetta 3.4 homology and loop-modeling applications to build *de novo* a region between residues F159 and L175 in our V1V2 CAP45 model (gray arrows; partial strand B and full strand C), without bias from the original PG9-bound starting template. The remodeled region contains an α-helix between residues K168 and L175 (magenta). (B) The helical conformation between residues K168 and L175 complexed with Fab CH58 (30) was superimposed with our remodeled-strand-C full V1V2 (dotted box in panel A). While the side chains presented small differences in their chi angles, the overall backbone conformation between the crystallized peptide (tan) and our model (magenta) superimposed well. (C) Surface representation of the remodeled V1V2 and mapped epitope residues (Fig. 4). Note that in the helical conformation, residues K168 and K169 would be located on the same face and in sufficient proximity to the integrin binding site that the V2i mAbs might be able to form direct contacts with them.

here assist in understanding the importance of maintaining particular hydrophobic amino acids at position 181.

The V2 integrin binding motif at positions 179 to 181 (LDI in most gp120 strains, but PDV in CAP45) has been proposed to bind α4β7 integrin on host cells in the early stages of viral infection (13, 17, 55), although this issue remains controversial (11). Our mutational data and those of Mayr et al. (33) suggest that the epitope of MAb 2158 and other V2i MAbs overlaps the integrin binding motif (Fig. 4) and that mutations at position D180 (D180G, D180S, and D180E) abrogate binding to MAb 2158. The experimental data, together with our computational analysis, suggest that most mutations of this residue do not induce conformational changes of the V2 structure. Taken together, these data indicate that the D180 side chain likely mediates direct contact with MAb 2158.

Current data have demonstrated that strand C of V1V2 can adopt different conformations. The crystal structures of the V2q MAbs PG9 and PG16 in complex with a scaffolded V1V2 have shown that the region between residues 170 and 176 forms strand C of the 4-stranded beta sheet (28). In contrast, recent epitope-complexed structures of V2p-specific MAbs CH58 and CH59, which were isolated from an RV144 vaccine recipient, suggest that this region also exists as a helix or a coil (30). There are several possible explanations for these differences: one is that the beta strand conformation is preferentially present in trimeric gp120, while the helical conformation preferentially exists in monomeric gp120 (30). We computationally constructed another model of V1V2, in which we removed all the atoms from the strand B-C region (positions 159 to 175) and built *de novo* a loop without the bias of any template structure (Fig. 6A). The remodeled region forms a helix between residues K168 and L175, which superimposes well with the helical epitope recognized by MAb CH58 (Fig. 6B). This alternative conformation shifts the position of K169 to the same exposed surface as that of the integrin binding site, which brings K169 to within 15 Å of V181, potentially part of the epitope recognized by MAb 2158, an intriguing possibility given that a match at position 169 was a correlate of reduced risk in RV144 (34). Another possibility is that tier 1 viruses preferentially harbor the helical conformation, while tier 2 viruses prefer the beta strand, a hypothesis which is consistent with the preferential neutralization of tier 2 viruses by MAb PG9 (24). It is also possible that inserting V1V2 into the protein G beta subunit (PDB entry 1FD6) scaffold stabilized its conformation for optimal binding to MAbs PG9 and PG16. In examining the crystal structures of the scaffolded V1V2, one finds that K168 can form a salt bridge with a glutamic acid on the 1FD6 scaffold. This contact with the scaffold may stabilize V1V2 in the PG9/PG16 binding conformation. Trimeric gp120 on the native virion may have such stabilizing factors, such that it preferentially harbors the epitopes recognized by V2q MAbs PG9 and PG16 in the quaternary Env structure (21, 22). When such stabilizing constraints are removed, the region for strand C in V1V2 may prefer the helical structure found in the complex of MAb CH58 with a V2 peptide, concurring with our computational modeling (Fig. 6). Together, these data suggest that strand C of V2 may adopt alternative conformations, and the loss of binding to MAb 2158 reported with the introduction of mutations at residues 168 and 169 in strand C may be due to conformational changes rather than direct antibody contacts.

Understanding the structural contributions of each residue in V2, the various conformations that V2 can assume, and the identities of the amino acids that interact with V2 antibodies will contribute to the selection and design of immunogens that can induce V2 antibodies with protective functions. Such immunogens may be trimeric envelopes, monomeric gp120, or recombinant epitope-scaffold immunogens, such as scaffolded V1V2s. The data presented above provide both modeling and binding data that address issues of structure, conformation, and antigenicity, and they provide a possible explanation for the findings from the RV144 sieve analysis that a mismatch of I181 in V2 leads to enhanced vaccine efficacy (34) and that different families of MAbs

specific for regions in strand C of V2 can recognize multiple conformations (28, 30). Together, these studies may help to lay the foundation for designing immunogens capable of inducing protective V2 antibodies.

ACKNOWLEDGMENTS

We thank Peter Kwong for plasmids containing scaffolded V1V2, Constance Williams and Timothy O'Neal for help with mAb production, Kevin Drew for help with using the Rosetta software package, and Yingkai Zhang for access to NYU's high-performance computing.

This work was supported in part by funds from the Department of Veterans Affairs, Veterans Health Administration, Office of Research and Development, and by NIH grants AI100151, AI084119, HL59725, and AI96946. B.S. was supported by NIH training grant GM088118. Beamline GM/CA at APS has been funded in whole or in part with federal funds from the National Cancer Institute (grant Y1-CO-1020) and the National Institute of General Medical Sciences (grant Y1-GM-1104). Use of the APS was supported by the U.S. Department of Energy, Basic Energy Sciences, Office of Science, under contract DE-AC02-06CH11357.

REFERENCES

1. **Rerks-Ngarm S, Pitisuttithum P, Nitayaphan S, Kaewkungwal J, Chiu J, Paris R, Premsri N, Namwat C, de Souza M, Adams E, Benenson M, Gurunathan S, Tartaglia J, McNeil JG, Francis DP, Stablein D, Birx DL, Chunsuttiwat S, Khamboonruang C, Thongcharoen P, Robb ML, Michael NL, Kunasol P, Kim JH.** 2009. Vaccination with ALVAC and AIDSVAX to prevent HIV-1 infection in Thailand. N. Engl. J. Med. **361:** 2209–2220. http://dx.doi.org/10.1056/NEJMoa0908492.
2. **Haynes BF, Gilbert PB, McElrath MJ, Zolla-Pazner S, Tomaras GD, Alam SM, Evans DT, Montefiori DC, Karnasuta C, Sutthent R, Liao HX, DeVico AL, Lewis GK, Williams C, Pinter A, Fong Y, Janes H, DeCamp A, Huang Y, Rao M, Billings E, Karasavvas N, Robb ML, Ngauy V, de Souza MS, Paris R, Ferrari G, Bailer RT, Soderberg KA, Andrews C, Berman PW, Frahm N, De Rosa SC, Alpert MD, Yates NL, Shen X, Koup RA, Pitisuttithum P, Kaewkungwal J, Nitayaphan S, Rerks-Ngarm S, Michael NL, Kim JH.** 2012. Immune-correlates analysis of an HIV-1 vaccine efficacy trial. N. Engl. J. Med. **366:**1275–1286. http://dx.doi.org/10.1056/NEJMoa1113425.
3. **Zolla-Pazner S, deCamp AC, Cardozo T, Karasavvas N, Gottardo R, Williams C, Morris DE, Tomaras G, Rao M, Billings E, Berman P, Shen X, Andrews C, O'Connell RJ, Ngauy V, Nitayaphan S, de Souza M, Korber B, Koup R, Bailer RT, Mascola JR, Pinter A, Montefiori D, Haynes BF, Robb ML, Rerks-Ngarm S, Michael NL, Gilbert PB, Kim JH.** 2013. Analysis of V2 antibody responses induced in vaccinees in the ALVAC/AIDSVAX HIV-1 vaccine efficacy trial. PLoS One **8:**e53629. http://dx.doi.org/10.1371/journal.pone.0053629.
4. **Stamatatos L, Wiskerchen M, Cheng-Mayer C.** 1998. Effect of major deletions in the V1 and V2 loops of a macrophage-tropic HIV type 1 isolate on viral envelope structure, cell entry, and replication. AIDS **14:** 1129–1139.
5. **Pinter A, Honnen WJ, He Y, Gorny MK, Zolla-Pazner S, Kayman SC.** 2004. The V1/V2 domain of gp120 is a global regulator of the sensitivity of primary human immunodeficiency virus type 1 isolates to neutralization by antibodies commonly induced upon infection. J. Virol. **78:**5205–5215. http://dx.doi.org/10.1128/JVI.78.10.5205-5215.2004.
6. **Israel ZR, Gorny MK, Palmer C, McKeating JA, Zolla-Pazner S.** 1997. Prevalence of a V2 epitope in clade B primary isolates and its recognition by sera from HIV-1-infected individuals. AIDS **11:**128–130.
7. **Gorny MK, Pan R, Williams C, Wang XH, Volsky B, O'Neal T, Spurrier B, Sampson JM, Li L, Seaman MS, Kong XP, Zolla-Pazner S.** 2012. Functional and immunochemical cross-reactivity of V2-specific monoclonal antibodies from HIV-1-infected individuals. Virology **427:**198–207. http://dx.doi.org/10.1016/j.virol.2012.02.003.
8. **Zolla-Pazner S, Cardozo T.** 2010. Structure-function relationships of HIV-1 envelope sequence-variable regions refocus vaccine design. Nat. Rev. Immunol. **10:**527–535. http://dx.doi.org/10.1038/nri2801.
9. **Karasavvas N, Billings E, Rao M, Williams C, Zolla-Pazner S, Bailer RT, Koup RA, Madnote S, Arworn D, Shen X, Tomaras GD, Currier JR, Jiang M, Magaret C, Andrews C, Gottardo R, Gilbert P, Cardozo TJ, Rerks-Ngarm S, Nitayaphan S, Pitisuttithum P, Kaewkungwal J, Paris R, Greene K, Gao H, Gurunathan S, Tartaglia J, Sinangil F, Korber BT, Montefiori DC, Mascola JR, Robb ML, Haynes BF, Ngauy V, Michael NL, Kim JH, de Souza MS, MOPH TAVEG Collaboration.** 2012. The Thai phase III HIV type 1 vaccine trial (RV144) regimen induces antibodies that target conserved regions within the V2 loop of gp120. AIDS Res. Hum. Retroviruses **28:**1444–1457. http://dx.doi.org/10.1089/aid.2012.0103.
10. **Pinter A.** 2007. Roles of HIV-1 Env variable regions in viral neutralization and vaccine development. Curr. HIV Res. **5:**542–553. http://dx.doi.org/10.2174/157016207782418470.
11. **Parrish NF, Wilen CB, Banks LB, Iyer SS, Pfaff JM, Salazar-Gonzalez JF, Salazar MG, Decker JM, Parrish EH, Berg A, Hopper J, Hora B, Kumar A, Mahlokozera T, Yuan S, Coleman C, Vermeulen M, Ding H, Ochsenbauer C, Tilton JC, Permar SR, Kappes JC, Betts MR, Busch MP, Gao F, Montefiori D, Haynes BF, Shaw GM, Hahn BH, Doms RW.** 2012. Transmitted/founder and chronic subtype C HIV-1 use CD4 and CCR5 receptors with equal efficiency and are not inhibited by blocking the integrin alpha4beta7. PLoS Pathog. **8:**e1002686. http://dx.doi.org/10.1371/journal.ppat.1002686.
12. **Haase AT.** 2005. Perils at mucosal front lines for HIV and SIV and their hosts. Nat. Rev. Immunol. **5:**783–792. http://dx.doi.org/10.1038/nri1706.
13. **Arthos J, Cicala C, Martinelli E, Macleod K, Van Ryk D, Wei D, Xiao Z, Veenstra TD, Conrad TP, Lempicki RA, McLaughlin S, Pascuccio M, Gopaul R, McNally J, Cruz CC, Censoplano N, Chung E, Reitano KN, Kottilil S, Goode DJ, Fauci AS.** 2008. HIV-1 envelope protein binds to and signals through integrin alpha4beta7, the gut mucosal homing receptor for peripheral T cells. Nat. Immunol. **9:**301–309. http://dx.doi.org/10.1038/ni1566.
14. **Cicala C, Martinelli E, McNally JP, Goode DJ, Gopaul R, Hiatt J, Jelicic K, Kottilil S, Macleod K, O'Shea A, Patel N, Van Ryk D, Wei D, Pascuccio M, Yi L, McKinnon L, Izulla P, Kimani J, Kaul R, Fauci AS, Arthos J.** 2009. The integrin alpha4beta7 forms a complex with cell-surface CD4 and defines a T-cell subset that is highly susceptible to infection by HIV-1. Proc. Natl. Acad. Sci. U. S. A. **106:**20877–20882. http://dx.doi.org/10.1073/pnas.0911796106.
15. **Nakamura GR, Fonseca DP, O'Rourke SM, Vollrath AL, Berman PW.** 2012. Monoclonal antibodies to the V2 domain of MN-rgp120: fine mapping of epitopes and inhibition of alpha4beta7 binding. PLoS One **7:**e39045. http://dx.doi.org/10.1371/journal.pone.0039045.
16. **Kopycinski J, Cheeseman H, Ashraf A, Gill D, Hayes P, Hannaman D, Gilmour J, Cox JH, Vasan S.** 2012. A DNA-based candidate HIV vaccine delivered via in vivo electroporation induces CD4 responses toward the alpha4beta7-binding V2 loop of HIV gp120 in healthy volunteers. Clin. Vaccine Immunol. **19:**1557–1559. http://dx.doi.org/10.1128/CVI.00327-12.
17. **Ansari AA, Reimann KA, Mayne AE, Takahashi Y, Stephenson ST, Wang R, Wang X, Li J, Price AA, Little DM, Zaidi M, Lyles R, Villinger F.** 2011. Blocking of alpha4beta7 gut-homing integrin during acute infection leads to decreased plasma and gastrointestinal tissue viral loads in simian immunodeficiency virus-infected rhesus macaques. J. Immunol. **186:**1044–1059. http://dx.doi.org/10.4049/jimmunol.1003052.
18. **Liu J, Bartesaghi A, Borgnia MJ, Sapiro G, Subramaniam S.** 2008. Molecular architecture of native HIV-1 gp120 trimers. Nature **455:**109–113. http://dx.doi.org/10.1038/nature07159.
19. **White TA, Bartesaghi A, Borgnia MJ, Meyerson JR, de la Cruz MJ, Bess JW, Nandwani R, Hoxie JA, Lifson JD, Milne JL, Subramaniam S.** 2010. Molecular architectures of trimeric SIV and HIV-1 envelope glycoproteins on intact viruses: strain-dependent variation in quaternary structure. PLoS Pathog. **6:**e1001249. http://dx.doi.org/10.1371/journal.ppat.1001249.
20. **Meyerson JR, White TA, Bliss D, Moran A, Bartesaghi A, Borgnia MJ, de la Cruz MJ, Schauder D, Hartnell LM, Nandwani R, Dawood M, Kim B, Kim JH, Sununu J, Yang L, Bhatia S, Subramaniam C, Hurt DE, Gaudreault L, Subramaniam S.** 2011. Determination of molecular structures of HIV envelope glycoproteins using cryo-electron tomography and automated sub-tomogram averaging. J. Vis. Exp. **58:**2770. http://dx.doi.org/10.3791/2770.
21. **Tran EE, Borgnia MJ, Kuybeda O, Schauder DM, Bartesaghi A, Frank GA, Sapiro G, Milne JL, Subramaniam S.** 2012. Structural mechanism of trimeric HIV-1 envelope glycoprotein activation. PLoS Pathog. **8:**e1002797. http://dx.doi.org/10.1371/journal.ppat.1002797.
22. **Lyumkis D, Julien JP, de Val N, Cupo A, Potter CS, Klasse PJ, Burton DR, Sanders RW, Moore JP, Carragher B, Wilson IA, Ward AB.** 2013. Cryo-EM structure of a fully glycosylated soluble cleaved HIV-1 envelope

trimer. Science **342:**1484–1490. http://dx.doi.org/10.1126/science.1245627.

23. **Julien JP, Cupo A, Sok D, Stanfield RL, Lyumkis D, Deller MC, Klasse PJ, Burton DR, Sanders RW, Moore JP, Ward AB, Wilson IA.** 2013. Crystal structure of a soluble cleaved HIV-1 envelope trimer. Science **342:**1477–1483. http://dx.doi.org/10.1126/science.1245625.
24. **Walker LM, Phogat SK, Chan-Hui PY, Wagner D, Phung P, Goss JL, Wrin T, Simek MD, Fling S, Mitcham JL, Lehrman JK, Priddy FH, Olsen OA, Frey SM, Hammond PW, Protocol G Principle Investigators, Kaminsky S, Zamb T, Moyle M, Koff WC, Poignard P, Burton DR.** 2009. Broad and potent neutralizing antibodies from an African donor reveal a new HIV-1 vaccine target. Science **326:**285–289. http://dx.doi.org/10.1126/science.1178746.
25. **Bonsignori M, Hwang KK, Chen X, Tsao CY, Morris L, Gray E, Marshall DJ, Crump JA, Kapiga SH, Sam NE, Sinangil F, Pancera M, Yongping Y, Zhang B, Zhu J, Kwong PD, O'Dell S, Mascola JR, Wu L, Nabel GJ, Phogat S, Seaman MS, Whitesides JF, Moody MA, Kelsoe G, Yang X, Sodroski J, Shaw GM, Montefiori DC, Kepler TB, Tomaras GD, Alam SM, Liao HX, Haynes BF.** 2011. Analysis of a clonal lineage of HIV-1 envelope V2/V3 conformational epitope-specific broadly neutralizing antibodies and their inferred unmutated common ancestors. J. Virol. **85:**9998–10009. http://dx.doi.org/10.1128/JVI.05045-11.
26. **Gorny MK, Stamatatos L, Volsky B, Revesz K, Williams C, Wang XH, Cohen S, Staudinger R, Zolla-Pazner S.** 2005. Identification of a new quaternary neutralizing epitope on human immunodeficiency virus type 1 virus particles. J. Virol. **79:**5232–5237. http://dx.doi.org/10.1128/JVI.79.8.5232-5237.2005.
27. **Moore PL, Gray ES, Sheward D, Madiga M, Ranchobe N, Lai Z, Honnen WJ, Nonyane M, Tumba N, Hermanus T, Sibeko S, Mlisana K, Abdool Karim SS, Williamson C, Pinter A, Morris L, CAPRISA 002 Study.** 2011. Potent and broad neutralization of HIV-1 subtype C by plasma antibodies targeting a quaternary epitope including residues in the V2 loop. J. Virol. **85:**3128–3141. http://dx.doi.org/10.1128/JVI.02658-10.
28. **McLellan JS, Pancera M, Carrico C, Gorman J, Julien JP, Khayat R, Louder R, Pejchal R, Sastry M, Dai K, O'Dell S, Patel N, Shahzad-ul-Hussan S, Yang Y, Zhang B, Zhou T, Zhu J, Boyington JC, Chuang GY, Diwanji D, Georgiev I, Kwon YD, Lee D, Louder MK, Moquin S, Schmidt SD, Yang ZY, Bonsignori M, Crump JA, Kapiga SH, Sam NE, Haynes BF, Burton DR, Koff WC, Walker LM, Phogat S, Wyatt R, Orwenyo J, Wang LX, Arthos J, Bewley CA, Mascola JR, Nabel GJ, Schief WR, Ward AB, Wilson IA, Kwong PD.** 2011. Structure of HIV-1 gp120 V1/V2 domain with broadly neutralizing antibody PG9. Nature **480:**336–343. http://dx.doi.org/10.1038/nature10696.
29. **Pancera M, Shahzad-Ul-Hussan S, Doria-Rose NA, McLellan JS, Bailer RT, Dai K, Loesgen S, Louder MK, Staupe RP, Yang Y, Zhang B, Parks R, Eudailey J, Lloyd KE, Blinn J, Alam SM, Haynes BF, Amin MN, Wang LX, Burton DR, Koff WC, Nabel GJ, Mascola JR, Bewley CA, Kwong PD.** 2013. Structural basis for diverse N-glycan recognition by HIV-1-neutralizing V1-V2-directed antibody PG16. Nat. Struct. Mol. Biol. **20:**804–813. http://dx.doi.org/10.1038/nsmb.2600.
30. **Liao HX, Bonsignori M, Alam SM, McLellan JS, Tomaras GD, Moody MA, Kozink DM, Hwang KK, Chen X, Tsao CY, Liu P, Lu X, Parks RJ, Montefiori DC, Ferrari G, Pollara J, Rao M, Peachman KK, Santra S, Letvin NL, Karasavvas N, Yang ZY, Dai K, Pancera M, Gorman J, Wiehe K, Nicely NI, Rerks-Ngarm S, Nitayaphan S, Kaewkungwal J, Pitisuttithum P, Tartaglia J, Sinangil F, Kim JH, Michael NL, Kepler TB, Kwong PD, Mascola JR, Nabel GJ, Pinter A, Zolla-Pazner S, Haynes BF.** 2013. Vaccine induction of antibodies against a structurally heterogeneous site of immune pressure within HIV-1 envelope protein variable regions 1 and 2. Immunity **38:**176–186. http://dx.doi.org/10.1016/j.immuni.2012.11.011.
31. **Bonsignori M, Pollara J, Moody MA, Alpert MD, Chen X, Hwang KK, Gilbert PB, Huang Y, Gurley TC, Kozink DM, Marshall DJ, Whitesides JF, Tsao CY, Kaewkungwal J, Nitayaphan S, Pitisuttithum P, Rerks-Ngarm S, Kim JH, Michael NL, Tomaras GD, Montefiori DC, Lewis GK, DeVico A, Evans DT, Ferrari G, Liao HX, Haynes BF.** 2012. Antibody-dependent cellular cytotoxicity-mediating antibodies from an HIV-1 vaccine efficacy trial target multiple epitopes and preferentially use the VH1 gene family. J. Virol. **86:**11521–11532. http://dx.doi.org/10.1128/JVI.01023-12.
32. **Gorny MK, Moore JP, Conley AJ, Karwowska S, Sodroski J, Williams C, Burda S, Boots LJ, Zolla-Pazner S.** 1994. Human anti-V2 monoclonal antibody that neutralizes primary but not laboratory isolates of human immunodeficiency virus type 1. J. Virol. **68:**8312–8320.
33. **Mayr LM, Cohen S, Spurrier B, Kong XP, Zolla-Pazner S.** 2013. Epitope mapping of conformational V2-specific anti-HIV human monoclonal antibodies reveals an immunodominant site in V2. PLoS One **8:**e70859. http://dx.doi.org/10.1371/journal.pone.0070859.
34. **Rolland M, Edlefsen PT, Larsen BB, Tovanabutra S, Sanders-Buell E, Hertz T, deCamp AC, Carrico C, Menis S, Magaret CA, Ahmed H, Juraska M, Chen L, Konopa P, Nariya S, Stoddard JN, Wong K, Zhao H, Deng W, Maust BS, Bose M, Howell S, Bates A, Lazzaro M, O'Sullivan A, Lei E, Bradfield A, Ibitamuno G, Assawadarachai V, O'Connell RJ, deSouza MS, Nitayaphan S, Rerks-Ngarm S, Robb ML, McLellan JS, Georgiev I, Kwong PD, Carlson JM, Michael NL, Schief WR, Gilbert PB, Mullins JI, Kim JH.** 2012. Increased HIV-1 vaccine efficacy against viruses with genetic signatures in Env V2. Nature **490:**417–420. http://dx.doi.org/10.1038/nature11519.
35. **Gorny MK, Xu JY, Gianakakos V, Karwowska S, Williams C, Sheppard HW, Hanson CV, Zolla-Pazner S.** 1991. Production of site-selected neutralizing human monoclonal antibodies against the third variable domain of the human immunodeficiency virus type 1 envelope glycoprotein. Proc. Natl. Acad. Sci. U. S. A. **88:**3238–3242. http://dx.doi.org/10.1073/pnas.88.8.3238.
36. **Teng NN, Lam KS, Calvo Riera F, Kaplan HS.** 1983. Construction and testing of mouse-human heteromyelomas for human monoclonal antibody production. Proc. Natl. Acad. Sci. U. S. A. **80:**7308–7312. http://dx.doi.org/10.1073/pnas.80.23.7308.
37. **Battye TG, Kontogiannis L, Johnson O, Powell HR, Leslie AG.** 2011. iMOSFLM: a new graphical interface for diffraction-image processing with MOSFLM. Acta Crystallogr. D Biol. Crystallogr. **67:**271–281. http://dx.doi.org/10.1107/S0907444910048675.
38. **Karplus PA, Diederichs K.** 2012. Linking crystallographic model and data quality. Science **336:**1030–1033. http://dx.doi.org/10.1126/science.1218231.
39. **Altschul SF, Gish W, Miller W, Myers EW, Lipman DJ.** 1990. Basic local alignment search tool. J. Mol. Biol. **215:**403–410.
40. **McCoy AJ, Grosse-Kunstleve RW, Adams PD, Winn MD, Storoni LC, Read RJ.** 2007. Phaser crystallographic software. J. Appl. Crystallogr. **40:**658–674. http://dx.doi.org/10.1107/S0021889807021206.
41. **Adams PD, Grosse-Kunstleve RW, Hung LW, Ioerger TR, McCoy AJ, Moriarty NW, Read RJ, Sacchettini JC, Sauter NK, Terwilliger TC.** 2002. PHENIX: building new software for automated crystallographic structure determination. Acta Crystallogr. D Biol. Crystallogr. **58:**1948–1954. http://dx.doi.org/10.1107/S0907444902016657.
42. **Emsley P, Cowtan K.** 2004. Coot: model-building tools for molecular graphics. Acta Crystallogr. D Biol. Crystallogr. **60:**2126–2132. http://dx.doi.org/10.1107/S0907444904019158.
43. **Fernandez-Recio J, Totrov M, Abagyan R.** 2002. Soft protein-protein docking in internal coordinates. Protein Sci. **11:**280–291. http://dx.doi.org/10.1110/ps.19202.
44. **An J, Totrov M, Abagyan R.** 2005. Pocketome via comprehensive identification and classification of ligand binding envelopes. Mol. Cell. Proteomics **4:**752–761. http://dx.doi.org/10.1074/mcp.M400159-MCP200.
45. **Raman S, Vernon R, Thompson J, Tyka M, Sadreyev R, Pei J, Kim D, Kellogg E, DiMaio F, Lange O, Kinch L, Sheffler W, Kim BH, Das R, Grishin NV, Baker D.** 2009. Structure prediction for CASP8 with all-atom refinement using Rosetta. Proteins **77**(Suppl 9)**:**89–99. http://dx.doi.org/10.1002/prot.22540.
46. **Kellogg EH, Leaver-Fay A, Baker D.** 2011. Role of conformational sampling in computing mutation-induced changes in protein structure and stability. Proteins **79:**830–838. http://dx.doi.org/10.1002/prot.22921.
47. **Reeves PJ, Callewaert N, Contreras R, Khorana HG.** 2002. Structure and function in rhodopsin: high-level expression of rhodopsin with restricted and homogeneous N-glycosylation by a tetracycline-inducible N-acetylglucosaminyltransferase I-negative HEK293S stable mammalian cell line. Proc. Natl. Acad. Sci. U. S. A. **99:**13419–13424. http://dx.doi.org/10.1073/pnas.212519299.
48. **Kabat EA, Wu TT.** 1991. Identical V region amino acid sequences and segments of sequences in antibodies of different specificities. Relative contributions of VH and VL genes, minigenes, and complementarity-determining regions to binding of antibody-combining sites. J. Immunol. **147:**1709–1719.
49. **Pancera M, McLellan JS, Wu X, Zhu J, Changela A, Schmidt SD, Yang Y, Zhou T, Phogat S, Mascola JR, Kwong PD.** 2010. Crystal structure of

PG16 and chimeric dissection with somatically related PG9: structure-function analysis of two quaternary-specific antibodies that effectively neutralize HIV-1. J. Virol. **84:**8098–8110. http://dx.doi.org/10.1128/JVI.00966-10.

50. **Pejchal R, Walker LM, Stanfield RL, Phogat SK, Koff WC, Poignard P, Burton DR, Wilson IA.** 2010. Structure and function of broadly reactive antibody PG16 reveal an H3 subdomain that mediates potent neutralization of HIV-1. Proc. Natl. Acad. Sci. U. S. A. **107:**11483–11488. http://dx.doi.org/10.1073/pnas.1004600107.
51. **Spurrier B, Sampson JM, Totrov M, Li H, O'Neal T, Williams C, Robinson J, Gorny MK, Zolla-Pazner S, Kong XP.** 2011. Structural analysis of human and macaque mAbs 2909 and 2.5B: implications for the configuration of the quaternary neutralizing epitope of HIV-1 gp120. Structure **19:**691–699. http://dx.doi.org/10.1016/j.str.2011.02.012.
52. **Qian B, Raman S, Das R, Bradley P, McCoy AJ, Read RJ, Baker D.** 2007. High-resolution structure prediction and the crystallographic phase problem. Nature **450:**259–264. http://dx.doi.org/10.1038/nature06249.
53. **Wang C, Bradley P, Baker D.** 2007. Protein-protein docking with backbone flexibility. J. Mol. Biol. **373:**503–519. http://dx.doi.org/10.1016/j.jmb.2007.07.050.
54. **Yu Y, Zhu J, Mi LZ, Walz T, Sun H, Chen J, Springer TA.** 2012. Structural specializations of alpha(4)beta(7), an integrin that mediates rolling adhesion. J. Cell Biol. **196:**131–146. http://dx.doi.org/10.1083/jcb.201110023.
55. **Tjomsland V, Ellegard R, Kjolhede P, Wodlin NB, Hinkula J, Lifson JD, Larsson M.** 2013. Blocking of integrins inhibits HIV-1 infection of human cervical mucosa immune cells with free and complement-opsonized virions. Eur. J. Immunol. **43:**2361–2372. http://dx.doi.org/10.1002/eji.201243257.